ADVANCES IN ATMOSPHERIC SCIENCES, VOL. 22, NO. 2, 2005, 300–312

Four-Dimensional Variational Data Assimilation Experiments for a Heavy Rain Case During the 2002 IOP in China

ZHANG Lin[1] (张 林) and NI Yunqi*[2] (倪允琪)

[1]*Department of Atmospheric Sciences, Nanjing University, Nanjing* 210093

[2]*State Key Laboratory of Sever Weather, Chinese Academy of Meteorological Sciences, Beijing* 100081

(Received 15 September 2003; revised 31 December 2004)

ABSTRACT

A heavy rainfall event along the mei-yu front during 22–23 June 2002 was chosen for this study. To assess the impact of the routine and additional IOP (intensive observation period) radiosonde observations on the mesoscale heavy rainfall forecast, a series of four-dimensional variational (4DVAR) data assimilation and model simulation experiments was conducted using nonhydrostatic mesoscale model MM5 and the MM5 4DVAR system. The effects of the intensive observations in the different areas on the heavy rainfall forecast were also investigated. The results showed that improvement of the forecast skill for mesoscale heavy rainfall intensity was possible from the assimilation of the IOP radiosonde observations. However, the impact of the IOP observations on the forecast of the rainfall pattern was not significant. Initial conditions obtained through the 4DVAR experiments with a 12-h assimilation window were capable of improving the 24-h forecast. The simulated results after the assimilation showed that it would be best to perform the intensive radiosonde observations in the upstream of the rainfall area and in the moisture passageway area at the same time. Initial conditions created by the 4DVAR led to the low-level moisture convergence over the rainfall area, enhanced frontogenesis and upward motion within the mei-yu front, and intensified middle- and high-level unstable stratification in front of the mei-yu front. Consequently, the heavy rainfall forecast was improved.

Key words: intensive radiosonde observations, four-dimensional variational assimilation

1. Introduction

Meteorological disasters are often caused by mesoscale severe storm systems, but the evolution of these systems and the interaction between the mesoscale systems and the synoptic-scale systems are not well understood. Therefore, how to improve short-range quantitative precipitation prediction remains a challenge. Numerical forecast of mesoscale weather systems has its own characteristics. The initial conditions (ICs) need to have more genesis and development information of the mesoscale systems. It is difficult to predict the mesoscale structures of these systems from the ICs without mesoscale details, especially when local factors play an important role.

Twice daily routine radiosounding is insufficient in spatial and temporal resolution to describe the structures of the mesoscale weather systems. With the development of satellite and radar remote sensing techniques, how to make good use of these non-conventional observations becomes an urgent task. The difficulties lie in the different nature of the data with different spatial and temporal resolutions. We should not only incorporate multi-time-level data in a scientific manner but also guarantee dynamic consistency between the initial conditions and the numerical model. The four-dimensional variational assimilation method (4DVAR) is a possibility.

4DVAR was applied firstly to one-dimensional models (Le Dimet and Talagrand, 1986), and then it was used in more sophisticated models (e.g., Thepaut and Courtier, 1991; Navon et al., 1992; Zou et al., 1993). At present, the global 4DVAR system, with physics ranging from simplified to improved and complex versions, has been developed at the European Centre for Medium-Range Weather Forecasts (ECMWF) (Rabier et al., 2000; Mahfouf and Rabier, 2000; Klinker et al., 2000), and at the National Cen-

*E-mail: niyunqi@cams.cma.gov.cn

ters for Environmental Prediction (NCEP) using the global spectral model and its "full-physics" adjoint model (Zou, et al., 2001).

In March 2002, the Japan Meteorological Agency implemented a mesoscale 4DVAR system with a 10-km resolution for operational numerical weather prediction. This is the first attempt in the world, and it has contributed to significant improvements in the forecast skill of heavy rainfall events.

The MM5 4DVAR system is based on the nonhydrostatic mesoscale model MM5. Zou and Kuo (1996) conducted 4DVAR precipitation data experiments using the MM5 4DVAR system. Guo et al. (2000) also performed a series of real-data assimilation experiments using the MM5 4DVAR system with a full physics adjoint. The encouraging results showed that the MM5 4DVAR system was able to reproduce the observed rainfall in terms of precipitation pattern and amount. Zhang et al. (2003) implanted a bogus vortex into the original initial field using the MM5 4DVAR system to improve the prediction of typhoon Herb.

In the 2002 field experiments, intensive observations were taken over the middle and lower reaches of the Yangtze River of China. At 0600 UTC 22 June, the radiosonde observations were collected at seven intensive observation stations (Fig. 1). We used the MM5 4DVAR system to perform assimilation experiments of the routine and intensive radiosonde observations and investigated the impact of the assimilated results on the heavy rainfall forecast and the effects of the intensive radiosonde observations.

The World Meteorological Organization (WMO) is now promoting the Observing System Research and Predictability Experiment (THORPEX). It is a ten-year long international research program. One of its objectives is to accelerate the improvements in the accuracy of numerical weather forecasts by enhancing the observing systems. Actually, data should be collected in specific areas at specific times for improving the numerical weather forecasts. This research topic known as "target observations" has been studied by many scientists in the world. Some studies are based on tangent-linear model integrations, while others are based on synoptic experience or on tracking potential vorticity anomalies (Szunyogh et al., 1999). In this study, we also investigated the effects of the observations in the certain areas selected for IOP observing fields on the heavy rainfall forecast through 4DVAR experiments. Due to the lack of real intensive radiosonde observations, all the additional experiments used NCEP re-analysis as pseudo-observations.

Section 2 gives a brief description of the MM5 model with the 4DVAR system and the experimental design. Section 3 describes the synoptic case chosen for this study, followed by the analyses of the experimental results in section 4. A detailed study of the pseudo-observations in the certain areas will be given in section 5. Our conclusions are given in section 6.

2. A brief description of the MM5 model with the 4DVAR system and experimental design

2.1 *MM5 model and 4DVAR system*

The mesoscale model MM5 with the 4DVAR system used in this study was developed by Pennsylvania State University (Penn State) and the National Center for Atmospheric Research (NCAR). A detailed description of MM5 can be found in Grell et al. (1994).

The MM5 4DVAR system includes MM5 Version 1, its tangent linear and adjoint models. The tangent linear and adjoint models were developed directly from the discrete MM5V1. This method avoids the difficulty arising from the derivation of tangent linear and adjoint equations from the original equations. The L-BFGS method was used in the minimization procedure. A detailed description of the MM5 4DVAR system can be found in Zou et al. (1997).

2.2 *Experimental design*

The triplex nested grid (Fig. 1) is used in the simulation experiments. The model domains consist of a 90-km grid (D01, grid size of 35×35), a 30-km grid (D02, grid size of 73×73), and a 10-km grid (D03, grid size of 91×91). There is a total of 23 layers in the vertical. Considering the lack of rainfall observation fields with 30-km or higher spatial resolution, all the results mentioned below come from the domain D02.

To reduce the computational expense and to overcome the difficulty of convergence in the minimization

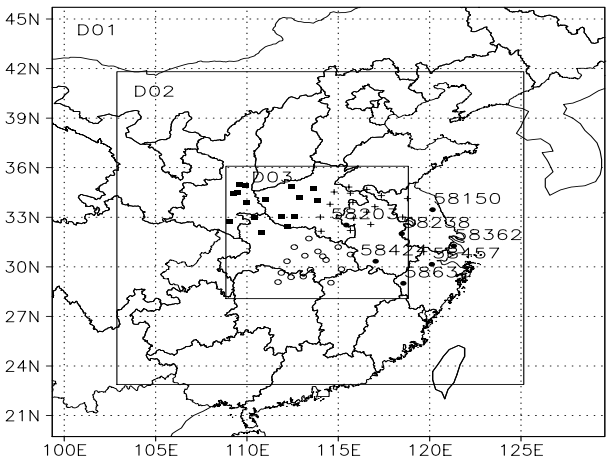

Fig. 1. The model domains. Black dots are the intensive sounding stations. Crosses, open circles and closed boxes indicate the test sounding stations.

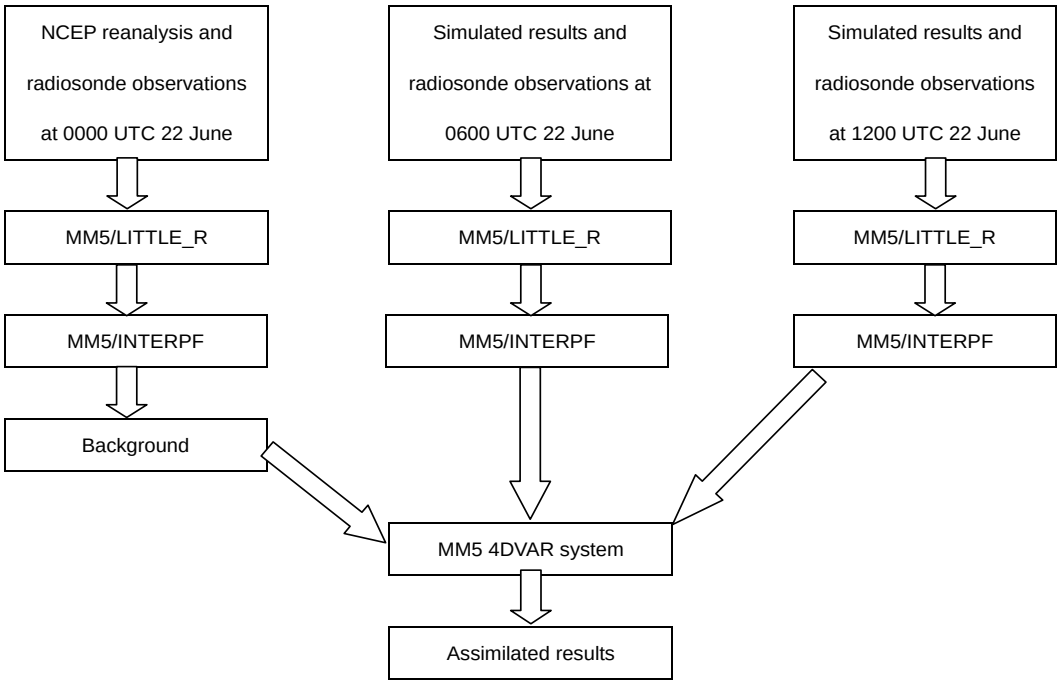

Fig. 2. The schematic diagram of the assimilation experiments. (The MM5/LITTLE_R program performs a single variable objective analysis and the MM5/INTERPF program handles the transformations to go from the analysis programs to the mesoscale model.)

procedure, the assimilation experiments are performed in the coarse domain D01 with 10 levels in the vertical. The ICs with a finer resolution used by the simulation experiments are obtained through the interpolation of the assimilated results. This kind of experimental design can take advantage of the nested domain configuration of MM5 (Zou et al., 1997).

First of all, the simulation experiment CTRL1 is conducted. CTRL1 is a standard 24-h forward model forecast starting at 0000 UTC 22 June 2002 without data assimilation. This experiment is used as a benchmark for the 4DVAR experiments. The ICs used by CTRL1 are obtained through objective analysis of the 100 radiosonde observations using NCEP reanalysis as the first guess. This is the standard procedure for initializing the MM5 modeling system. Then the simulated results of CTRL1 are used as the first guess to perform the objective analysis of the routine and intensive radiosonde observations at 0600 UTC and 1200 UTC 22 June. We use wind, temperature, specific humidity and pressure perturbation data from objective analysis of the radiosonde observations at 0000 UTC, 0600 UTC and 1200 UTC 22 June to perform the four-dimensional variational data assimilation experiments. Therefore we do not directly assimilate the radiosonde data with 4DVAR but the objective analysis of the radiosonde observations (Fig. 2).

In general, the cost function used in the assimilation can be expressed as

$$\begin{aligned} J(X) =& (X_0 - X_\mathrm{b})^\mathrm{T} W_\mathrm{b} (X_0 - X_\mathrm{b}) \\ &+ \sum_{i=1}^{n} [X(t_i) - X_{\mathrm{obs}}(t_i)]^\mathrm{T} \\ &\times W_X [X(t_i) - X_{\mathrm{obs}}(t_i)] \,. \end{aligned} \tag{2.1}$$

Here, X_0 represents the model wind, temperature, specific humidity and pressure perturbation at the initial time; X_b represents the background; W_b is the weighting matrix for the background term; $X(t_i)$ represents the model variables at the time t_i; $X_{\mathrm{obs}(t_i)}$ represents the objective analysis of wind, temperature, specific humidity and pressure perturbation at the time t_i.

Since the objective analysis of wind, temperature, specific humidity and pressure perturbation are used as observations, no interpolation operator is included in (2.1). W_b and W_X should be the inverse of the objective analysis error covariance matrix. Here, they are simply based on the radiosonde observation error variances described by Parrish and Derber (1992). The observation-error variances of wind and temperature are defined at six levels beforehand, such as 1000 hPa, 700 hPa, 500 hPa, 300 hPa, 100 hPa, 50 hPa (Table 1). Since MM5 uses terrain-following coordinates and flux form governing equations, some conversions are implemented to obtain appropriate weights based on

the radiosonde observation error statistics and the surface reference pressure (Guo et al., 2000). For pressure perturbation and vertical velocity, the weights are calculated as the inverse of the squared maximum differences between the observations at two time levels. The specification of the weighting matrix is a complicated issue for variational data assimilation, which needs further study and is beyond the scope of this study. It should be pointed out that the method used in this study is experimental and the error variance of relative humidity is also determined empirically to obtain the successful results.

Six assimilation experiments are conducted, all of which use a 12-h assimilation window from 0000 to 1200 UTC 22 June. There are 100 routine radiosonde stations in the model domain D01, seven of which performed the intensive observation at 0600 UTC 22 June. The background fields used by the assimilation experiments are the same as the initial condition of CTRL1. The observations used by the assimilation experiments are shown in Table 2.

3. Synoptic situation during 22–23 June 2002

A mesoscale heavy rainfall event on the Mei-yu front that occurred in the middle and lower reaches of the Yangtze River during 22–23 June 2002 was chosen for this study. Brief description of the rainfall process and the synoptic situation is given as follows:

At 0000 UTC 22 June, the weak short wave trough moved eastward and the ridge of the western Pacific subtropical high (WPSH) was located along 24°N in the vicinity of 120°E at 500 hPa 120°E. The heavy rainfall during 0000–1200 UTC 22 June was concentrated in the east of Sichuan Province, the north of Hubei Province, and the south and east of Henan Province. The maximum 12-h rainfall in the south of Henan Province was over 100 mm (Fig. 3a).

At 1200 UTC 22 June, a shear line formed at 850 hPa over the north of Anhui Province and the south and east of Henan Province. It developed and maintained by 0000 UTC 23 June. The ascending motion in front of the trough and the shear line was responsible for the heavy rainfall in the south of Henan Province, the north of Anhui Province and Jiangsu Province. A maximum 12-h rainfall of 140 mm was located in the south of Henan Province (Fig. 3b).

During 0000–1200 UTC 23 June, the rainfall systems dissipated gradually. The range of the rainfall area in the south of Henan Province and the west of Anhui Province reduced and the maximum 12-h rainfall was only 40 mm (Fig. 3c).

Table 1. Observation-error variances.

	1000 hPa	700 hPa	500 hPa	300 hPa	100 hPa	50 hPa
Wind (m s^{-1})	1.4	2.4	2.8	3.4	2.5	2.7
Temperature (K)	1.8	1.3	1.3	2.0	3.1	4.0
Relative humidity			2% (all levels)			

Table 2. Observations used in four-dimensional variational (FDVAR) assimilation experiments.

	Time		
Name	0000 UTC 22	0600 UTC 22	1200 UTC 22
FDVAR 1	100 routine radiosondes	none	99 routine radiosondes
FDVAR 2	100 routine radiosondes	7 intensive radiosondes	99 routine radiosondes
FDVAR 3	100 routine radiosondes	16 test radiosondes in the rainfall area	99 routine radiosondes
FDVAR 4	100 routine radiosondes	16 test radiosondes in the moisture passageway to the south of the rainfall area	99 routine radiosondes
FDVAR 5	100 routine radiosondes	16 test radiosondes upstream of the rainfall area	99 routine radiosondes
FDVAR 6	100 routine radiosondes	32 test radiosondes used by FDVAR 4 and FDVAR 5	99 routine radiosondes

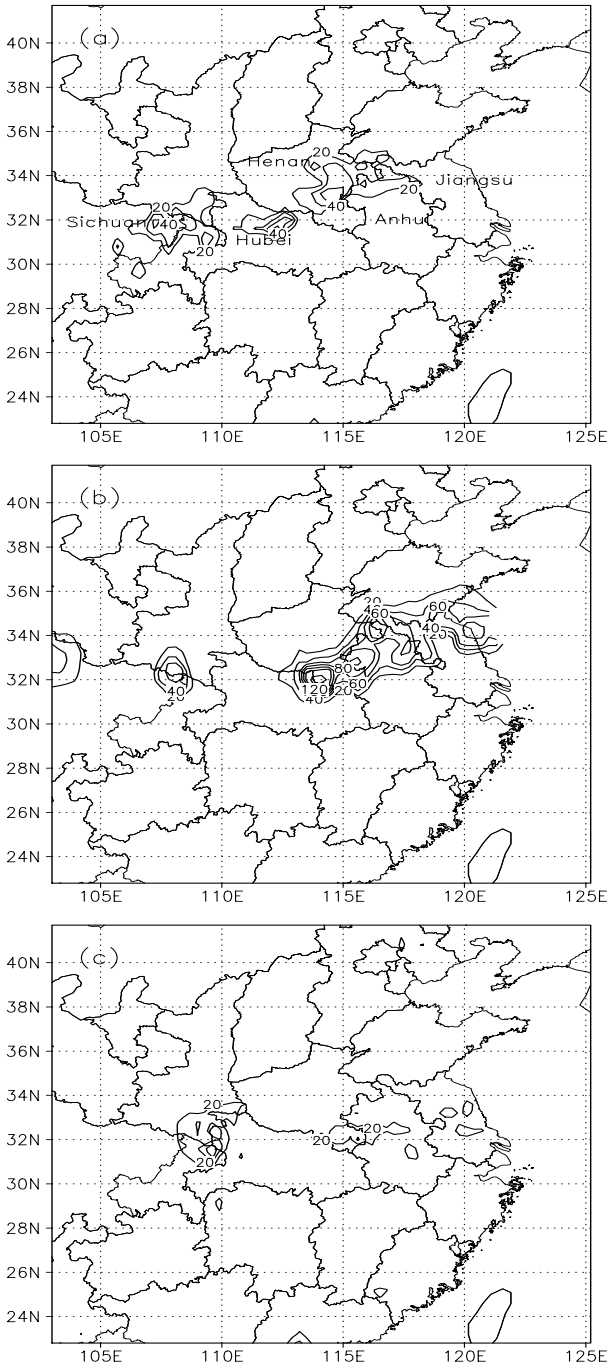

Fig. 3. The observed 12-h rainfall ending at (a) 1200 UTC 22, (b) 0000 UTC 23, and (c) 1200 UTC 23 June 2002 (contour interval is 20 mm).

Figure 4 shows the observed 24-h rainfall during 0000 UTC 22 June–0000 UTC 23 June 2002. Most of the strong rainfall was concentrated in the north of Hubei Province, the south and east of Henan Province, and the north of Anhui Province with a maximum 24-h accumulation of over 180 mm, except for the relatively

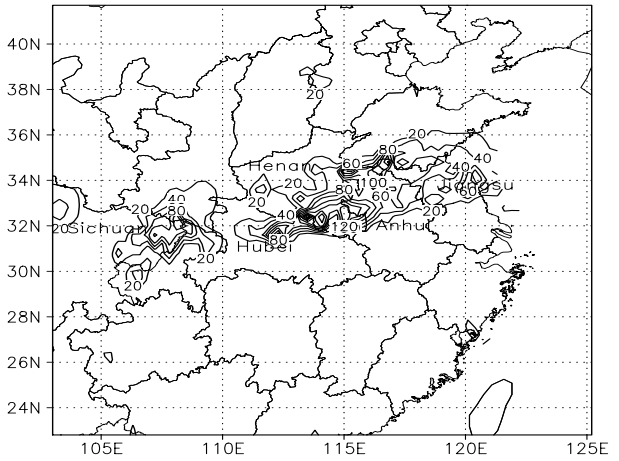

Fig. 4. The observed 24-h rainfall during 0000 UTC 22 June–0000 UTC 23 June 2002 (contour interval is 20 mm).

smaller rainfall area in the east of Sichuan Province with a maximum 24-h accumulation of 100 mm.

4. The impact of the intensive radiosonde observations during the 2002 field experiment on the mesoscale heavy rainfall forecast

To assess the impact of the intensive radiosonde observations during the 2002 field experiment on the mesoscale heavy rainfall forecast, two simulation experiments named ASSIM1 and ASSIM2 were conducted using the MM5V3 model. The initial conditions used by ASSIM1 and ASSIM2 come from the results of assimilation experiments FDVAR1 and FDVAR2 respectively.

4.1 *The performance of the minimization procedure*

In our assimilation experiments, the maximum number of iterations was set at 20. The cost function and the norm of the gradient decreased well for both 4DVAR experiments. Figure 5 gives the variations of the cost function and the norm of the gradient with respect to the number of iterations for FDVAR2. It is evident that the minimization procedure is convergent.

4.2 *Simulated rainfall results*

Figure 6 shows the simulated 12-h rainfall during the assimilation period of 0000–1200 UTC 22 June 2002. Without 4DVAR, the experiment CTRL1 did not capture the observed heavy rainfall centers. The simulated rainfall had a lower amount than the observed. However, both ASSIM1 and ASSIM2 were able

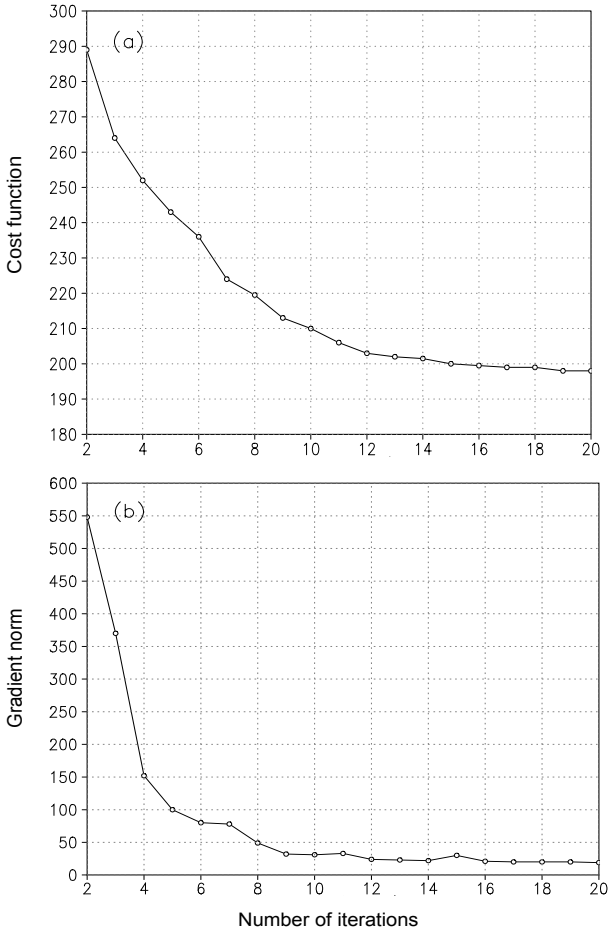

Fig. 5. (a) Cost function J and (b) norm of the gradient G with respect to the number of iterations for FDVAR2.

to improve the forecast skill for the heavy rainfall, especially in the south of Henan Province, but with a slightly higher amount as shown in Figs. 6b and 6c.

Figure 7 shows the subsequent simulated 12-h rainfall ending at 0000 UTC 23 June. The simulated rainfall from CTRL1 was poor both in rainfall intensity and its coverage. And ASSIM1 did not have a higher forecast skill compared with CTRL1. It failed to produce the heavy rainfall in the south of Henan province. However, ASSIM2 gave the best forecast of the heavy rainfall amount in this area using the intensive observations during the field experiment.

Moreover, we compared the observed 6-h rainfall in Xinyang City of Henan Province at 32.13°N, 114.05°E with the simulated results at the same location. During 0600 UTC 22 June–1200 UTC 23 June, the mesoscale rainfall process in Xinyang was observed. At 1800 UTC 22 June, the maximum 6-h rainfall reached 91 mm. CTRL1 failed to simulate this maximum rainfall intensity. After the assimilation of

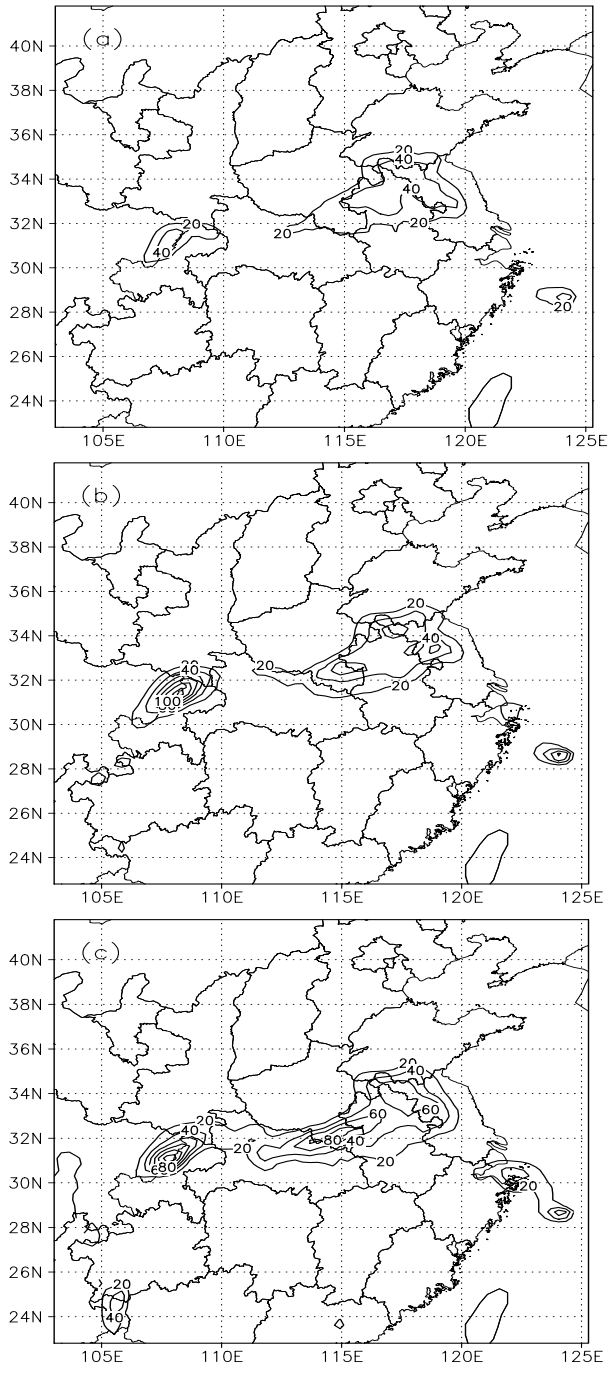

Fig. 6. The simulated 12-h rainfall during 0000–1200 UTC 22 June 2002 from (a)CTRL1, (b)ASSIM1, and (c) ASSIM2 (contour interval is 20 mm).

the radiosonde observations, the variations of the simulated rainfall from both ASSIM1 and ASSIM2 were closer to the observed. At 1800 UTC 22 June, the simulated 6-h rainfall was enhanced to a value of 30 mm instead of 9.2 mm without data assimilation (Fig. 8).

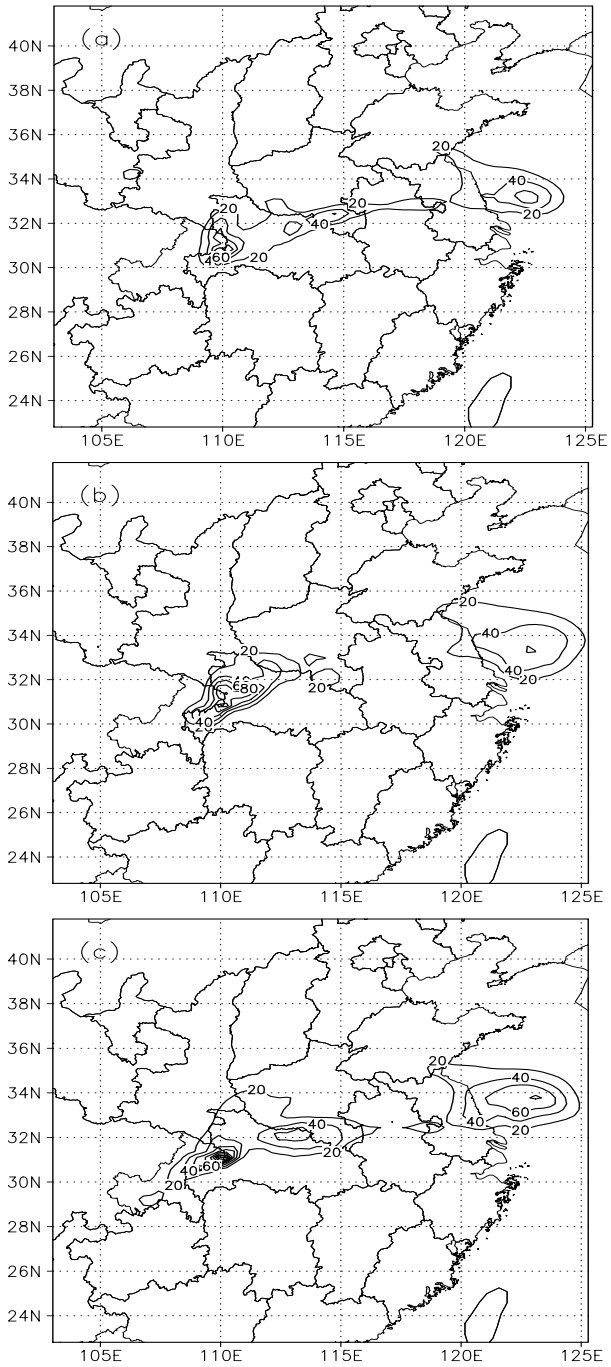

Fig. 7. The simulated 12-h rainfall during 1200 UTC 22 June–0000 UTC 23 June 2002 from (a) CTRL1, (b) ASSIM1, and (c) ASSIM2 (contour interval is 20 mm).

We calculated the threat score for all three experiments within the region of 29°N–36°N, 112°E–121.5°E. The results for the precipitation thresholds of 25 mm, 50 mm, and 100 mm are presented in Fig. 9. When the threshold value was 25 mm, the scores for the three experiments were all above 0.6. This suggested that all the experiments reproduced the 24-h rainfall at the right location. However, the threat score of ASSIM1 was zero for the 100 mm threshold value. It is apparent that ASSIM1 failed to predict the heavy rainfall of over 100 mm. The threat score of ASSIM2 increased by 0.19 and 0.22 for the 50 mm and 100 mm threshold values respectively in comparison with CTRL1. The improvement on the heavy rainfall forecast was obvious by the assimilation of the intensive radiosonde observations.

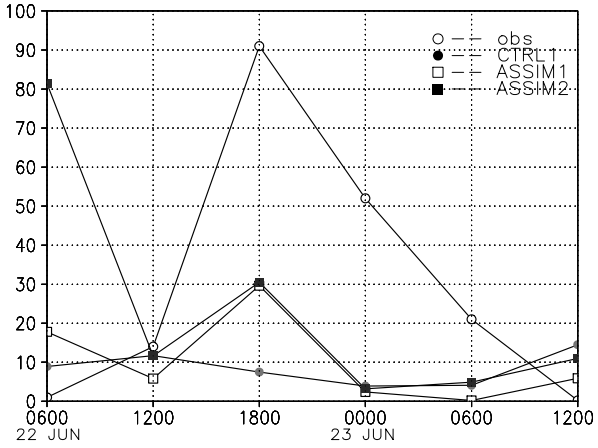

Fig. 8. Variations of the 6-h rainfall in Xinyang of Henan Province during 0600 UTC 22 June–0000 UTC 23 June (open circles: observation; closed circles: CTRL1; open panes: ASSIM1; closed panes: ASSIM2).

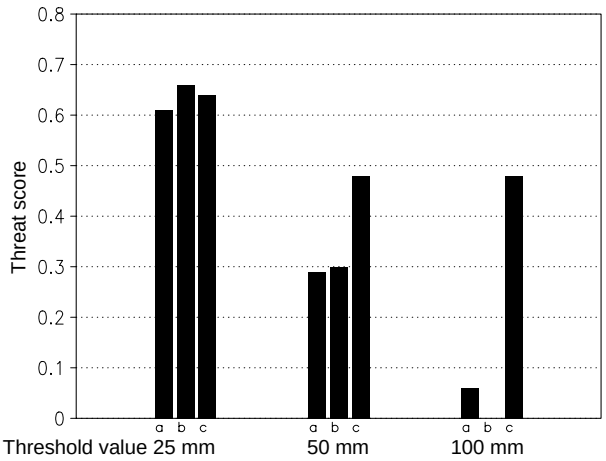

Fig. 9. The threat score of 24-h rainfall during 0000 UTC 22 June–0000 UTC 23 June within the region of 29°–36°N, 112°–121.5°E for (a) CTRL1, (b) ASSIM1, and (c) ASSIM2.

As presented in the comparison between the observed and the simulated rainfall, only seven intensive radiosonde observations were used in ASSIM2 and the heavy rainfall forecast was improved. The impact of the intensive observations during the field experiment

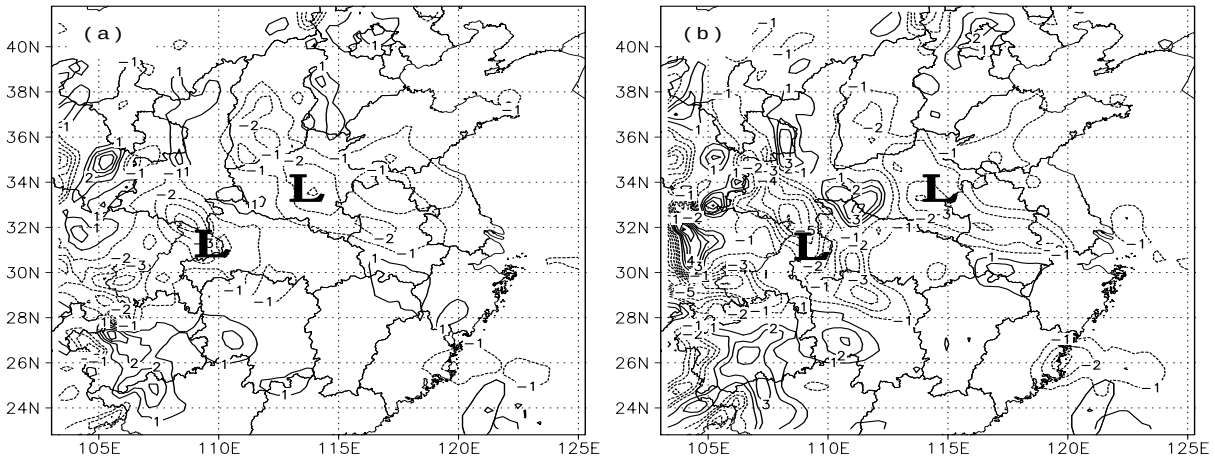

Fig. 10. The averaged moisture flux divergence $\nabla(\boldsymbol{V}q)$ for 1000 hPa–600 hPa at 0000 UTC 22 June (a) CTRL1, and (b) ASSIM2 (units in 10^{-7} s^{-1}).

on the mesoscale heavy rainfall forecast was remarkable.

4.3 *The improvement in the initial conditions resulting from the assimilation of the int ensive radiosonde observations*

As discussed in section 4.2, the ICs resulting from the assimilation of intensive radiosonde observations improved the mesoscale heavy rainfall forecast. Naturally, a question can be asked. Which modifications to the ICs made by 4DVAR led to the improved forecast? To answer this question, we examined the difference fields of several variables in the initial conditions between CTRL1 and ASSIM2. They are moisture advection, vertical motion and unstable stratification, which are crucial for the genesis and development of the heavy rainfall system.

There were two centers of moisture flux convergence in the low level whose locations were consistent with those of the observed rainfall centers (Fig. 10a). The maximum averaged moisture flux convergence for 1000 hPa–600 hPa reached -4×10^{-7} s^{-1} and -3×10^{-7} s^{-1} respectively. After the assimilation, they were enhanced up to values as large as -6×10^{-7} s^{-1} and -4×10^{-7} s^{-1} respectively (Fig. 10b). The enhanced low-level moisture convergence contribution was responsible for the moisture transport during the heavy rainfall event.

As mentioned in section 3, the ascending motion in front of the trough and the shear line resulted in the heavy rainfall during 22–23 June 2002. Figure 11 indicates the meridional-vertical cross section of the streamline and quasi-equivalent potential temperature θ_{se} along 114°E from CTRL1 and ASSIM2 at 0000 UTC 22 June. The warm and moist northward flow ascended along the mei-yu front in the low level. The upward motion over the rainfall area reached the maximum intensity at 300 hPa (Fig. 11a). There were subsidences of the air streams on both the south and north of the ascending flow. The descending flow at 26°N entrained and enhanced the upward motion over the rainfall area at 500 hPa. Without 4DAVR, the maximum speeds of the upward and downward motion were 20 cm s^{-1} and –8 cm s^{-1} respectively. However they reached 28 cm s^{-1} and –10 cm s^{-1} respectively by the adjustments of the assimilation experiment. These modifications created a favorable environment for the development of the convective systems.

There was a θ_{se} dense area around 34°N, namely a mei-yu front area, which extended to 650 hPa and tilted slightly northward (Fig. 11a). An interesting result is that it moved southward to 32°N and had a higher density after the assimilation (Fig. 11b). As shown in the meridional-vertical cross section of the difference fields of θ_{se} between ASSIM2 and CTRL1 along 114°E (Fig. 12), the dense area with the positive value was located around 31°N. In the layer from 850 hPa to 300 hPa over the south of the rainfall area, θ_{se} was enhanced and $\partial\theta_{se}/\partial p$ was positive for ASSIM2. The maximum adjustment of $\partial\theta_{se}/\partial p$ was 0.02 K hPa^{-1}. The results were similar in the difference fields of θ_{se} between ASSIM2 and ASSIM1 (Fig. 13). The maximum difference of θ_{se} between ASSIM2 and ASSIM1 over the south of the rainfall area was 4 K at 850 hPa. These results suggested that the unstable stratification was enhanced at the middle and high levels in front of the mei-yu front after the assimilation. We analyzed the meridional-vertical cross sections of the temperature and moisture at the same location (not shown) and found that the adjustments of the moisture were responsible for the changes of θ_{se}. After

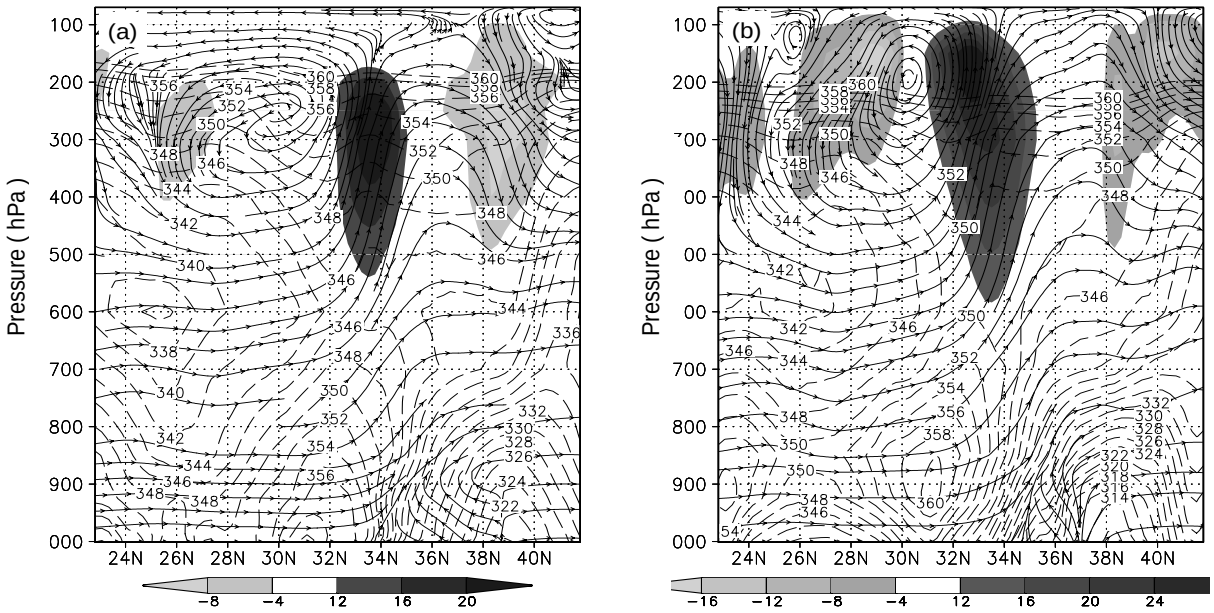

Fig. 11. The meridional-vertical sections of the streamline and quasi-equivalent potential temperature θ_{se} along 114°E at 0000 UTC 22 June (long dashes depict θ_{se} in K; shaded areas indicate the vertical velocity in cm s^{-1}) (a) CTRL1, and (b) ASSIM2.

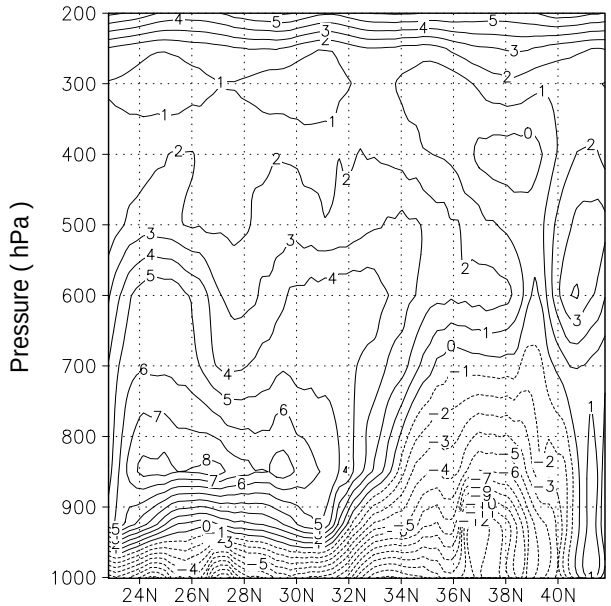

Fig. 12. The meridional-vertical section of the difference fields of the quasi-equivalent potential temperature θ_{se} between ASSIM2 and CTRL1 along 114°E at 0000 UTC 22 June (units in K).

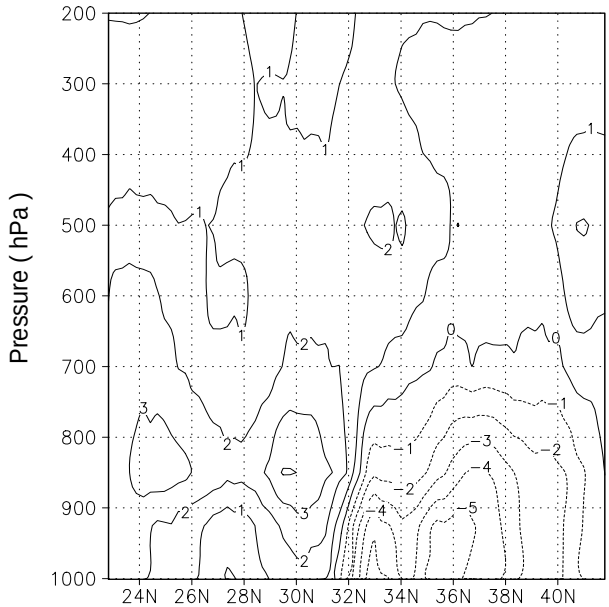

Fig. 13. The meridional-vertical section of the difference fields of the quasi-equivalent potential temperature θ_{se} between ASSIM2 and ASSIM1 along 114°E at 0000 UTC 22 June (units in K).

the assimilation of the intensive radiosonde observations, the moisture in front of the mei-yu front was enhanced and the situation was opposite behind the mei-yu front. Consequently, the difference in the moisture fields was increased in between the south and the north of mei-yu front. These modifications not only favored the development of the northward-slanting ascending flow in front of the mei-yu front but also increased the positive feedback between the moist physical process enhancing frontogenesis and the development of the

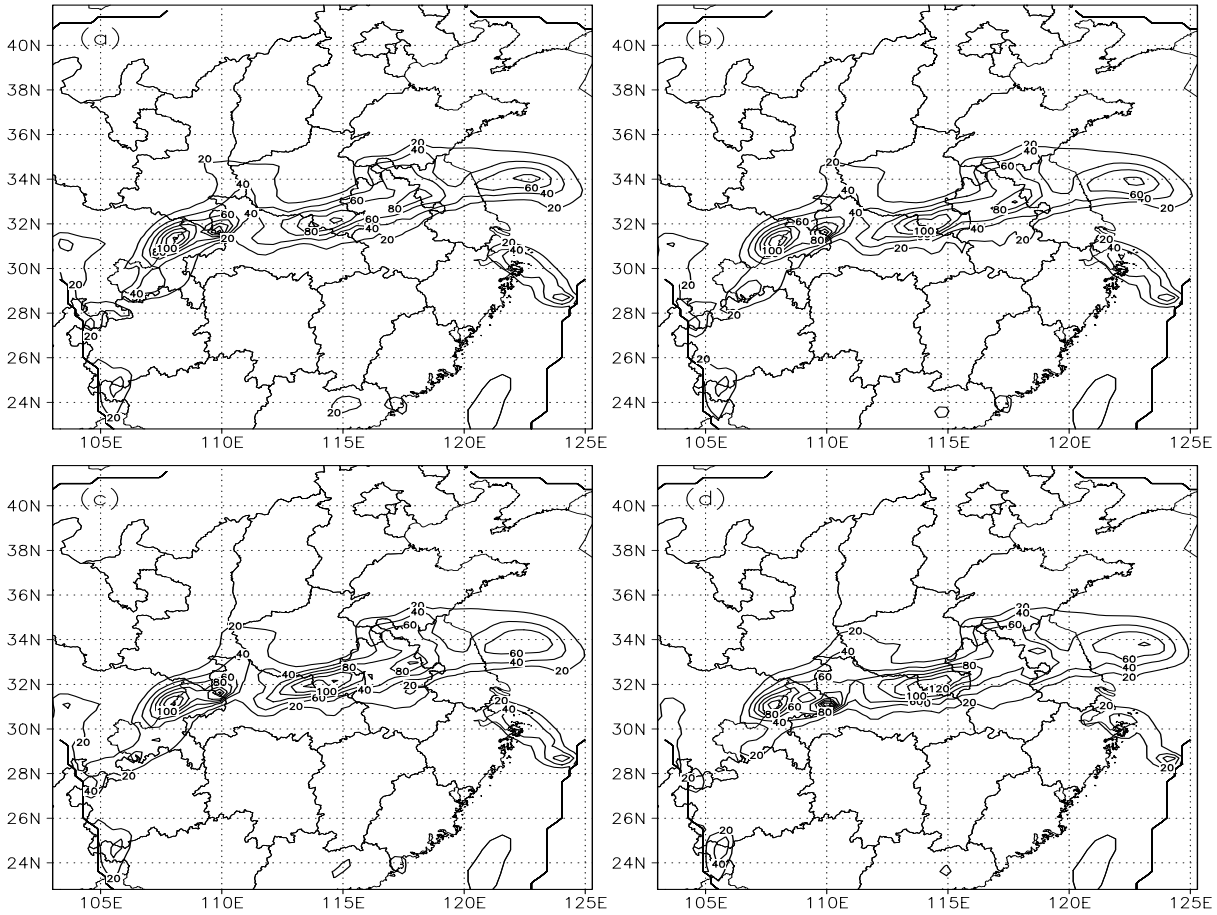

Fig. 14. The simulated 24-h rainfall during 0000 UTC 22 June–0000 UTC 23 June from (a)ASSIM3 (b) ASSIM4, (d) ASSIM5, and (d) ASSIM6. (contour interval is 20 mm).

strong convective system on the mei-yu front.

5. The simulation research on the selection of sensitive areas for IOP radiosonde data assimilation

There were only 7 radiosonde stations whose observations were used by the assimilation experiments. The locations of the stations were far away from the rainfall area. Would the heavy rainfall forecast after the assimilation of the radiosonde observations be improved further if the radiosonde stations were located in other areas? How do we select the intensive observing area to efficiently improve the heavy rainfall forecast? To investigate this issue, we performed four additional assimilation experiments, which were named FDVAR3, FDVAR4, FDVAR5 and FDVAR6.

We chose three regions for this study, located in the rainfall area (32°–35°N, 114°–119°E, on the south of the rainfall area 29°–32°N, 115°–116°E, and in the upstream of the rainfall area 32°–35°N, 109°–114°E (the crosses, open circles and closed squares as shown in Fig. 1). There were 16 test intensive stations in each area. Due to the lack of real observations, we attempted to perform a linear interpolation of NCEP reanalysis data to provide the pseudo-observations for the test stations at 0600 UTC 22 June. We have checked the quality of the pseudo-observations using the real radiosonde observations at 0600 UTC and 1200 UTC. The error variances of the pseudo-observations provided from NCEP re-analyzed data were mostly smaller than those of the simulated results from CTRL1 at the same time. The assimilation strategies of FDVAR3, FDVAR4, FDVAR5 and FDVAR6 were the same as those of FDVAR2 except that the observations at 0600 UTC 22 June came from the NCEP reanalysis instead of the 7 real radiosonde observations. Using the assimilated results from FDVAR3, FDVAR4, FDVAR5 and FDVAR6, we respectively performed the simulation experiments ASSIM3, ASSIM4, ASSIM5 and ASSIM6 and investigated the impact of the pseudo-observations in the areas men-

tioned above on the heavy rainfall forecast.

Figure 14 shows the simulated 24-h rainfall from ASSIM3, ASSIM4, ASSIM5 and ASSIM6 using the pseudo-observations the different areas. The two main observed rainfall areas, one around 31.8°N, 108°E and the other around 32°N, 114°E were both well reproduced. Considering the intensity of the simulated heavy rainfall, the results of ASSIM4 were superior to those of ASSIM3 but worse than those of ASSIM5. ASSIM6 performed best in forecasting the heavy rainfall. The maximum simulated 24-h rainfall of ASSIM6 was over 150 mm in the south of Henan Province.

Figure 15 shows the threat score of the 24-h rainfall during 0000 UTC 22 June–0000 UTC 23 June within the region of 29°N–36°N, 112°E–121.5°E for ASSIM3, ASSIM4, ASSIM5 and ASSIM6. It is clear that when the threshold values were 25 mm and 50 mm, the scores for the four experiments were all above 0.64 and 0.46 respectively. When the threshold value was 100 mm, ASSIM4 had a greater forecast skill than ASSIM3, but worse than ASSIM5. And ASSIM6 gave the best forecast skill of heavy rainfall. These results suggested that the pseudo-observations both in the upstream of the rainfall area and in the moisture passageway were valuable to the mesoscale heavy rainfall forecast.

As discussed earlier, the assimilated results using the radiosonde observations during 0000–1200 UTC 22 June were capable of improving the 24-h rainfall forecast during 0000 UTC 22 June–0000 UTC 23 June. Furthermore, we performed the simulation experiment CTRL2. It was initiated by the objective analysis of 99 radiosonde observations at 1200 UTC using the results of CTRL1 at 1200 UTC as the first guess. We wanted to see if 4DVAR would do a better job than it would for the 24-h forecast during 1200 UTC 22 June–1200 UTC 23 June.

We compared the 24-h rainfall of CTRL2 with that of ASSIM6 during 1200 UTC 22June–1200 UTC 23 June. Though the maximum 24-h rainfall reached 80 mm over the eastern areas of Sichuan Province, the

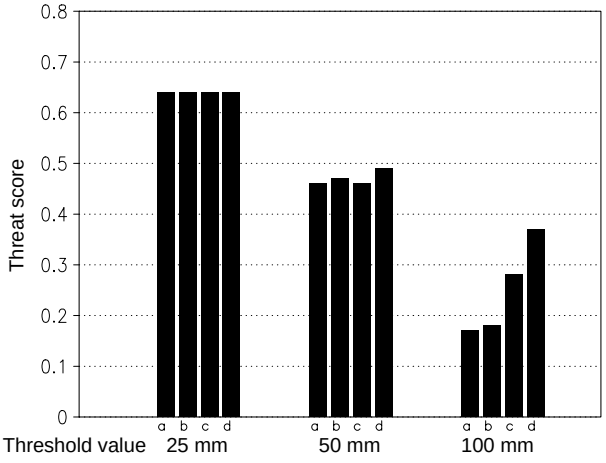

Fig. 15. The threat score of 24-h rainfall during 0000 UTC 22 June–0000 UTC 23 June within the region of 29°N–36°N, 112°E–121.5°E for a ASSIM3, b ASSIM4, c ASSIM5, and d ASSIM6.

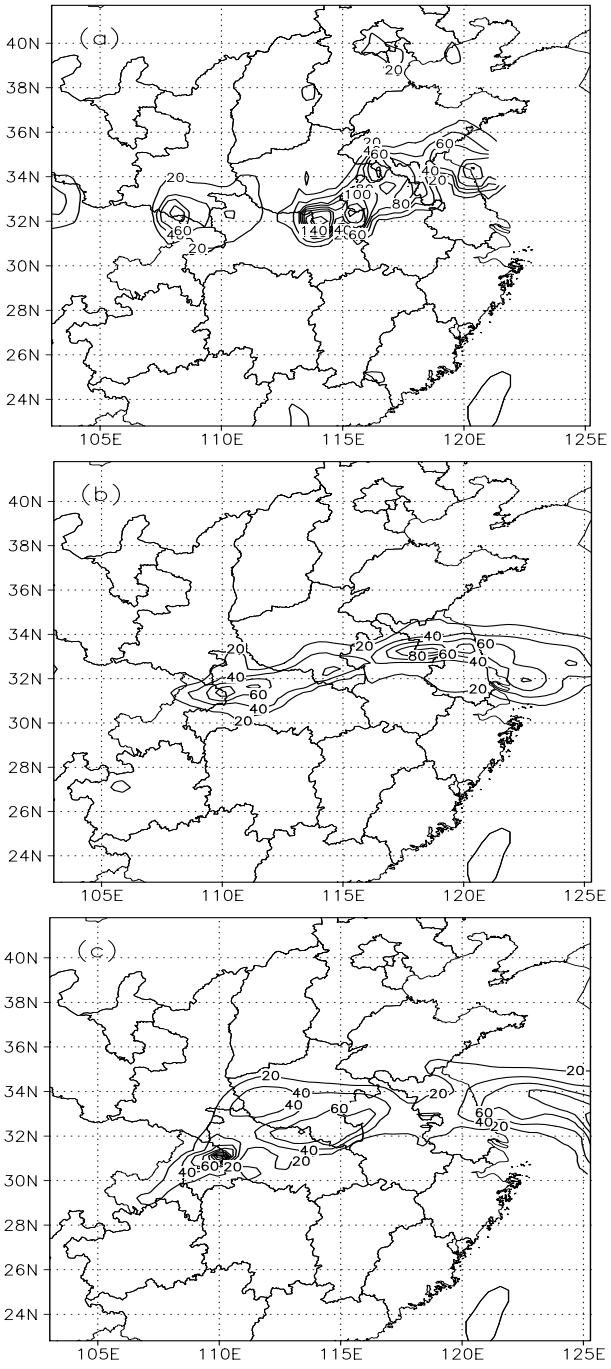

Fig. 16. The 24-h rainfall during 1200 UTC 22 June–1200 UTC 23 June 2002 from (a) observations, (b) CTRL2, and (c) ASSIM6 (contour interval is 20 mm).

observed heavy rainfall was still concentrated in the south of Henan Province with a maximum 24-h accumulation of over 160 mm during 1200 UTC 22 June–1200 UTC 23 June (Fig. 16a). Generally speaking, CTRL2 captured the main features of the observed heavy rainfall in terms of the intensity and location in the east of Sichuan Province, but it failed to simulate the heavy rainfall in the south of Henan Province. The maximum simulated rainfall in this area was only 80 mm and the range of the rain belt was smaller than the observed (Fig. 16b). However, the results from ASSIM6 were closer to the observed in the south of Henan Province (Fig. 16c). Figure 17 shows the threat score of 24-h rainfall during 1200 UTC 22 June–1200 UTC 23 June within the region of 29°N–36°N, 112°E–121.5°E for CTRL2 and ASSIM6. When the threshold values were 25 mm and 50 mm, the scores for the results of ASSIM6 increased by 0.04 and 0.06 respectively. These results suggested that the assimilated results with an assimilation window from 0000 UTC to 1200 UTC 22 June were superior to the objective analysis at 1200 UTC 22 June for the forecast of the 24-h rainfall during 1200 UTC 22 June–1200 UTC 23 June.

6. Conclusions and discussions

We performed four-dimensional variational data assimilation experiments using 100 routine radiosonde observations at 0000 UTC, 7 intensive radiosonde observations at 0600 UTC, and 99 routine radiosonde observations at 1200 UTC 22 June 2002. The impact of the ICs obtained through the assimilation experiments on the mesoscale heavy rainfall forecast was examined. The effects of intensive observations in different areas on the heavy rainfall forecast were also investigated.

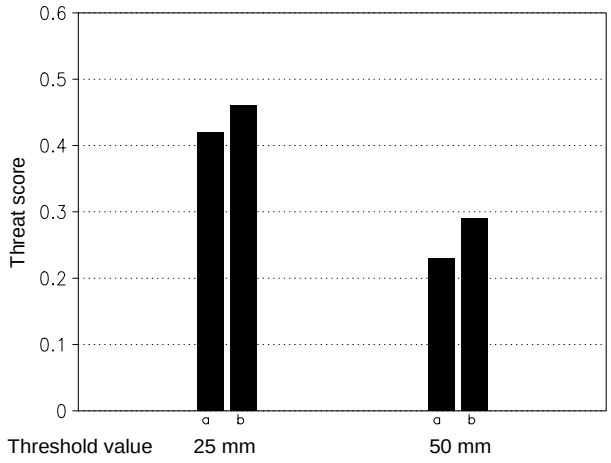

Fig. 17. The threat score of 24-h rainfall during 1200 UTC 22 June–1200 UTC 23 June within the region of 29°N–36°N, 112°E–121.5°E for a CTRL2, and b ASSIM6.

The ICs obtained through the 4DVAR experiments were capable of improving the mesoscale heavy rainfall forecast, especially the forecast of the heavy rainfall amount. But the impact on the forecast of the rainfall pattern was limited. The assimilated results using three-time-level observations were better than those using two-time-level observations. The initial conditions created by the 4DVAR experiments intensified the low-level moisture convergence, enhanced the frontogenesis and the upward motion on the mei-yu front, and adjusted the middle- and high-level unstable stratification in front of the mei-yu front to improve the heavy rainfall forecast.

The simulated results after the assimilation showed that it was best to perform the intensive observation in the upstream of the rainfall area and in the moisture passageway area to the south of the rainfall area at the same time.

The assimilated results with a 12-h assimilation window were able to improve the 24-h forecast after the ending time of the assimilation window.

Because the radiosonde observations do not have a sufficient resolution and since the computational conditions are limited, the 4DVAR experiments were performed with only a 90-km resolution. The assimilated results were unable to extract the mesoscale information from the observations. Further study is needed to perform the assimilation experiments of the satellite and radar data with higher resolution.

In section 5, NCEP reanalysis data were used to provide pseudo-observations at the test radiosonde stations. But this strategy is not satisfactory for mesoscale models. The better way to do this is maybe to use the high-resolution simulated results with better quality. And the quality of the pseudo-observations should be checked by the intensive mesoscale observations. These problems should be investigated in the future research.

Acknowledgments. The authors wish to thank Jia Pengqun for his comments on the manuscript. This work was funded by the National Key Fundamental Research Project "Research on the Formation Mechanism and the Prediction Theory of Hazardous Weather over China" (G1998040906-12).

REFERENCES

Andersson, E., J. Pailleux, J.-N. Thepaut, J. R. Eyre, A. P. McNally, G. A. Kelly, and P. Courtier, 1994: Use of cloud-cleared radiances in three/four dimensional variational data assimilation. *Quart. J. Roy. Meteor. Soc.*, **120**, 627–653.

Grell, Georg A., J. Dudhia, and D. R. Stauffer, 1994: A Description of the Fifth-Generation Penn State/NCAR Mesoscale Model (MM5). NCAR Tech. Note NCAR/TN-398+STR, 138pp. [Available from National Center for Atmospheric Research, P. O. Box 3000, Boulder, CO 80307-3000.]

Guo, Y.-R., Y.-H. Kuo, J. Dudhia, D. Parsons, and C. Rocken, 2000: Four-dimensional variational data assimilation of heterogeneous mesoscale observations for a strong convective case. *Mon. Wea. Rev.*, **128**, 619–643.

Klinker, E., F. Rabier, G. Kelly, and J.-F. Mahfouf, 2000: The ECMWF operational implementation of four-dimensional variational assimilation. Part III: Experimental results and diagnostics with operational configuration. *Quart. J. Roy. Meteor. Soc.*, **126**, 1191–1215.

Le Dimet, F.-X., and O. Talagrand, 1986: Variational algorithms for analysis and assimilation of meteorological observations: Theoretical aspects. *Tellus*, **38A**, 97–110.

Lorenc, A. C., 1997: Development of an operational variational assimilation scheme. *J. Meteor. Soc. Japan*, **75**(1B), 339–346.

Mahfouf, J.-F., and F. Rabier, 2000: The ECMWF operational implementation of four-dimensional variational assimilation. Part II: Experimental results with improved physics. *Quart. J. Roy. Meteor. Soc.*, **126**, 1171–1190.

Navon, I. M., X. Zou., J. Derber, and J. Sela, 1992: Variational data assimilation with an adiabatic version of the NMC spectral model. *Mon. Wea. Rev.*, **120**, 1433–1446.

Parrish, D. F., and John C. Derber, 1992: The National Meteorological Center's spectral statistical-interpolation analysis system. *Mon. Wea. Rev.*, **120**, 1747–1763.

Rabier, F., H. Jarvinen, E. Klinker, J.-F. Mahfouf, and A. Simmons, 2000: The ECMWF operational implementation of four-dimensional variational assimilation. Part I: Experimental results with simplified physics. *Quart. J. Roy. Meteor. Soc.*, **126**, 1143–1170.

Szunyogh, I., Z. Toth, R. E. Morss, S. J. Majumdar, B. J. Etherton, and C. H. Bishop, 1999: The Effect of Targeted Dropsonde Observations during the 1999 Winter Storm Reconnaissance Program. *Mon. Wea. Rev.*, **198**, 3520–3537.

Thepaut, J. N., and P. Courtier, 1991: Four-dimensional variational data assimilation using the adjoint of a multilevel primitive equation model. *Quart. J. Roy. Meteor. Soc.*, **117**, 1225–1254.

Zhang Xiaoyan, Wang Bin, Ji Zhongzhen, Qingnong Xiao, and Zhang Xin, 2003: Initialization and simulation of a typhoon using 4-dimensional variational data assimilation—Research on Typhoon Herb (1996). *Adv. Atmos. Sci.*, **20**(4), 612–622.

Zou, X., F. Vandenberghe, M. Pondeca, and Y.-H. Kuo, 1997: Introduction to adjoint techniques and the MM5 adjoint modeling system. NCAR Technical Note, NCAR/TN-435+STR, 110pp. [Available from National Center for Atmospheric Research, P. O. Box 3000, Boulder, CO 80307-3000.]

Zou, X, I. M. Navon, and J. G. Sela, 1993: Variational data assimilation with moist threshold processes using the NMC spectral model. *Tellus*, **45A**, 370–387.

Zou, X., and Y.-H. Kuo, 1996: Rainfall assimilation through an optimal control of initial and boundary conditions in a limited-area mesoscale model. *Mon. Wea. Rev.*, **124**, 2859–2882.

Zou, X., H. Liu, J. Derber, J. G. Sela, R. Treadon, I. M. Navon, and B. Wang, 2001: Four-dimensional variational data assimilation with a diabatic version of the NCEP global spectral model: System development and preliminary results. *Quart. J. Roy. Meteor. Soc.*, **127**, 1095–1122.

Zupanski, D., 1993: The effect of discontinuities in the Betts-Miller cumulus convection scheme on four dimensional data assimilation. *Tellus*, **45A**, 511–524.

Zupanski, D., and F. Mesinger, 1995: Four-dimensional variational assimilation of precipitation data. *Mon. Wea. Rev.*, **123**, 1112–1127.